JOURNAL OF MATERIALS SCIENCE 17 (1982) 406–416

A study of the effects of annealing, zinc diffusion and copper diffusion on the defect structure of silicon-doped gallium arsenide

P. W. HUTCHINSON,* R. K. BALL
Department of Physical Metallurgy and Science of Materials, University of Birmingham, P.O. Box 363, Birmingham, UK

Transmission electron microscopy has been employed to study as-received, annealed, zinc-diffused and copper-diffused silicon-doped GaAs. The results on the as-received material show that the defect structure is dependent on the silicon doping level, with small perfect and faulted loops being present at high doping levels. The results of the annealing study on heavily doped material show that the size and density of the loop structure is strongly dependent on the temperature and type of loop. This behaviour has been interpreted in terms of previous work on the variation of the point-defect populations and free-carrier concentration with annealing temperature. The effect of zinc diffusion on the defect structure of heavily Si-doped GaAs has been found to be very similar to that observed after equivalent diffusions into Te-doped GaAs and is explained with reference to these results. The differences between the two cases are thought to be mainly due to the amphoteric nature of silicon in GaAs. The diffusion of copper has been found to result in large increases in the perfect and faulted loop areas. This, it is suggested, is due to the mechanism of copper diffusion in GaAs and the effect on point-defect populations of in-diffusing a p-type dopant into n-type material.

1. Introduction

Transmission electron microscopy (TEM) studies of as-received Si-doped GaAs have revealed a microdefect structure whose density and composition appears to be strongly dependent on the silicon doping level. The results of Darby [1] and Darby *et al.* [2] suggest that below a carrier concentration of approximately 3.5×10^{18} cm^{-3} only dislocation lines ($< 10^3$ cm^{-2}) are observed in Si-doped substrates, whereas above this carrier concentration a high density of small, prismatic dislocation loops (20–50 nm) and a low density of large faulted loops ($\sim 1\,\mu$m diameter) exist. The density of these microdefects is reported to increase with increasing silicon doping. Some support for these results comes from the investigations of Narayanan and Kachare [3] who found that GaAs Si-doped to 4×10^{19} cm^{-3} contained a high density of small perfect loops and a few large stacking faults, while material doped to 10^{18} cm^{-3} exhibited only grown-in dislocations ($< 10^4$ cm^{-2}). Narayanan and Kachare [3] also investigated the effects of vacuum annealing on their material. They reported that if material doped to 4×10^{19} cm^{-3} was annealed at 1100° C for 15 min and then quenched, it exhibited a microstructure virtually devoid of microdefects. Subsequent re-annealing, however, at between 600 and 850° C produced perfect and faulted loops. The natures of the small perfect and large faulted loops in Si-doped GaAs were given by Narayanan and Kachare [3] as edge-type and vacancy with Burger's vectors of $a/2\langle 1\,1\,0\rangle$, and extrinsic, respectively.

Darby *et al.* [2] have also examined the effect of zinc diffusion in Si-doped substrates and have reported a diffusion-induced defect structure

*Present address: Cossor Electronics Limited, The Pinnacles, Elizabeth Way, Harlow CM19 5BB, UK

0022–2461/82/020406–11$3.10/0

which is dependent on the doping level. In the present investigation TEM has been used to examine the defects present in as-received Si-doped GaAs and to observe the change in defect structure after vacuum annealing, zinc diffusion and copper diffusion.

2. Experimental method

Two single-crystal (1 0 0) slices, A and B, taken from a crystal grown by a horizontal gradient freeze technique, were used in these investigations. The precise level of the Si-doping was not known; however, comparisons with the measured carrier concentrations [4] and total silicon concentrations [5] of adjacent or nearby slices from the same crystal, suggest that slice A would have a carrier concentration varying from between 1.7×10^{18} cm^{-3} to 2.3×10^{18} cm^{-3}, and slice B a carrier concentration varying from between 2.7×10^{18} cm^{-3} to 3.3×10^{18} cm^{-3} and a total silicon concentration in excess of 5×10^{18} cm^{-3}.

The two as-received slices were initially given an A–B etch [6] prior to cutting into 3 mm diameter discs. Heat treatments were carried out in sealed, evacuated (5×10^{-6} torr), vitreosil ampoules (approximately 6 mm in diameter and 60 mm long) and after annealing were quickly cooled to room temperature by a water quench. Diffusion specimens were initially ground and polished on successively finer abrasives down to 0.05 μm alumina and then chemically polished in a 2% bromine in methanol solution to remove the damaged layer. Diffusions were performed in sealed, evacuated (5×10^{-6} torr), vitreosil ampoules (approximately 6 mm in diameter and 60 mm long) which were necked to keep the specimens and the weighed source separate. In the case of zinc diffusion the source end of the ampoule was water-quenched on removal from the furnace to minimize vapour deposition on the specimen surface. In the case of copper diffusion the whole ampoule was water-quenched.

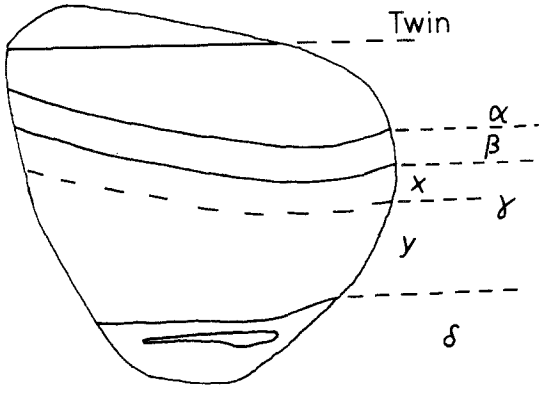

Figure 1 Schematic representation of the regions revealed on slice B after an A–B etch.

Planar TEM specimens were prepared by etching both faces in a 2% bromine-in-methanol solution. Transverse specimens were prepared using the method outlined by Ball *et al.* [7]. Examination was made using an EM7 high-voltage electron microscope and a Philips EM400 fitted with EDAX facilities.

3. Results

3.1. As-received and annealed material

Fig. 1 is a schematic representation of Slice B indicating the several different defect zones revealed by the A–B etch in the as-received material. Similar results were obtained by Stirland [8] on adjacent slices from the same crystal. Zones α, β and δ were visible to the naked eye as cloudy regions with β being less cloudy than the other two. Examination under an optical microscope revealed a high density of pits in zones α and δ and, on average, a lower density in β. Optical microscopy also revealed that zone γ could be subdivided into two regions X and Y. Region Y was virtually free of pits while in X the pit density increased from zero at the X–Y boundary to a maximum at the X–β boundary.

Several specimens from each zone were examined in the as-received state and after various annealing treatments. The results of these experiments on specimens in region α are summarized in Fig. 2. Fig. 2a shows a typical area from an as-received specimen in region α. The principal defects observed were:

(a) a relatively low density of large {1 1 1} faulted defects, about 0.7 to 1 μm in diameter, often multi-layered and occasionally complex, being associated with intersecting perfect loops;

(b) small perfect loops on {1 1 0} planes up to 0.1 μm in diameter;

(c) small {1 1 1} stacking faults of about the same size. Weak-beam microscopy shows that some are circular and some are roughly triangular in shape.

The combined density of the small loops was estimated at 4.3×10^{12} cm^{-3}. Annealing at 600° C for 6 to 17.5 h produced a defect structure as in

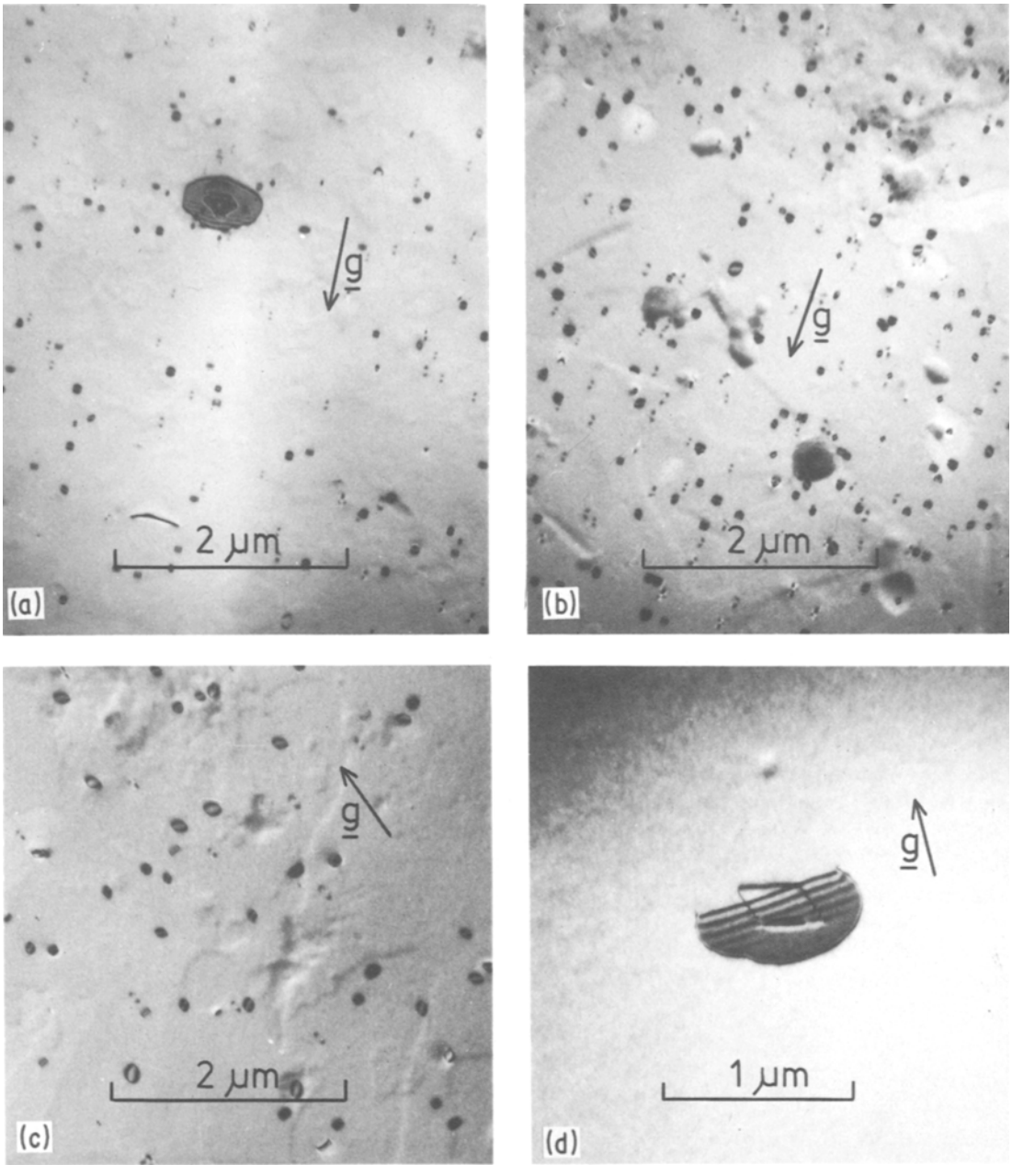

Figure 2 Variation of the size and density of the loop structure in region α with annealing temperature. (a) As-received, g 2 2 0, **B** [0 0 1], (800 kV); (b) 600° C, 17 h, g 2 $\bar{2}$ 0, **B** [0 0 1], (800 kV); (c) 800° C, 17 h, g 2 2 0, **B** [0 0], (800 kV); (d) 950° C, 17 h, g $\bar{2}$ 2 0, **B** [0 0 1], (800 kV).

Fig. 2b. The large stacking faults were, as far as could be estimated, unaffected but the combined density of the small perfect and faulted loops rose to an estimated value of 6.7×10^{12} cm^{-3}. Annealing at 800° C for 17 h produced no noticeable effect on the large stacking faults but the size of the small perfect and faulted loops rose while their combined density fell (2.7×10^{12} cm^{-3}) in relation to the as-received and 600° C annealed specimens (Fig. 2c). Annealing at 890° C for 4.5 h again has no discernible effect on the large stacking faults while the combined density of the smaller loops is similar to that in material annealed at 800° C. However, the average size of the small faulted loops appears to have fallen in relation to the 800° C anneal while the perfect loops are approxi-

TABLE I Estimates variation in loop sizes and area in region α with annealing temperature

Temperature (° C)	Average diameter of small stacking faults (nm)	Average diameter of perfect loops (nm)	Density of small faulted loops (cm^{-3})	Density of perfect loops (cm^{-3})	Small faulted loop area ($cm^2\ cm^{-3}$)	Perfect loop area ($cm^2\ cm^{-3}$)
As-received	53	52	3.7×10^{12}	3.2×10^{11}	84	7
600	62	64	5.7×10^{12}	1.0×10^{12}	180	35
714*	89	75	2.2×10^{12}	1.4×10^{12}	140	67
800	95	100	1.7×10^{12}	9.4×10^{11}	130	80
865*	65	68	1.2×10^{12}	2.0×10^{12}	42	76
890	59	107	8.2×10^{11}	1.3×10^{12}	25	130
950	~ 0	500 (edge length)	~ 0	1.3×10^{9}	~ 0	3
850 + copper	86	140	1.2×10^{13}	3.5×10^{12}	740	800
950 + copper	690 (large stacking faults)	207 (edge length)	4.8×10^{11} (large stacking faults)	1.2×10^{11}	1300 (large stacking faults)	44

*Estimates taken from the annealed bulk of zinc-diffused specimens.

mately the same size as those examined after the 800° C anneal. In specimens annealed at 950° C for 17 h no background of small, perfect or faulted loops was observed. Instead the defect structure consisted of large stacking faults, which appeared unaffected by the anneal, and a very low density of large (edge length 0.5 μm) parallelogram-shaped perfect loops (Fig. 2d). Specimens annealed at 1060° C for 20 min and quenched revealed only a low density of large stacking faults.

The results of the annealing experiments in region α are summarized in Table I. These results show that there is a marked difference between the behaviour of the small perfect and small faulted loops with annealing temperature.

Region β exhibited a low density of large, complex stacking faults ($\leqslant 1\,\mu$m in diameter) when examined in the as-received state. They were invariably multilayered and associated with a cluster of small perfect and faulted loops, as illustrated in Fig. 3a. No background of small loops, either perfect or faulted, was observed. However, annealing at 600° C for 6 h, while not visibly affecting the large stacking faults, did produce a background of small, perfect and faulted loops (Fig. 3b), though with a lower density ($1.7 \times 10^{12}\ cm^{-3}$) than that observed in equivalently heat-treated specimens from region α. Specimens annealed at 800° C for 17 h, however, showed no such background of small loops and,

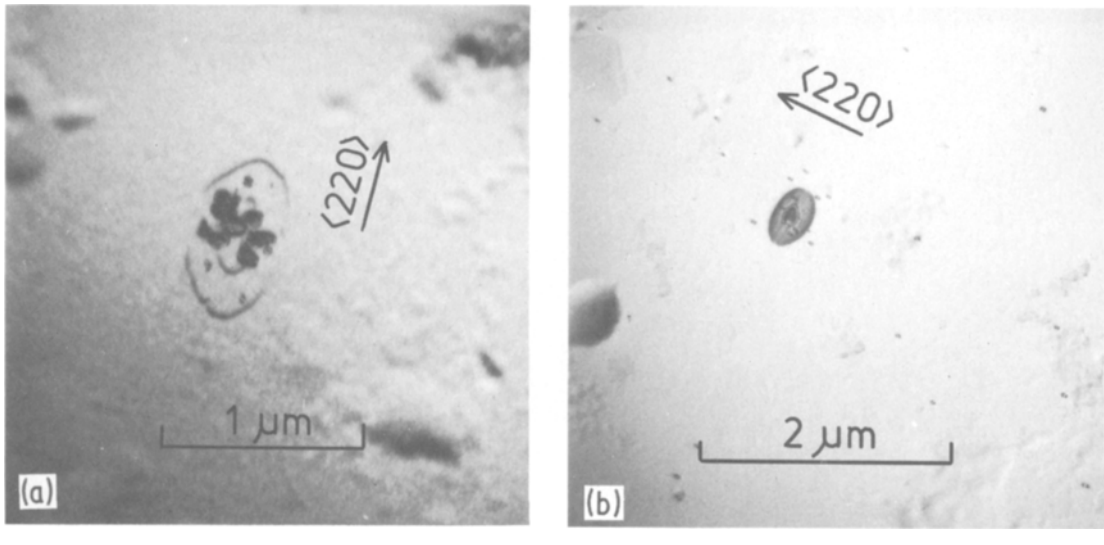

Figure 3 Variation of the dislocation structure in region β with annealing. (a) As-received, g 2 2 0, B [0 0 1], (800 kV). (b) 600° C, 6 h, g $\bar{2}$ 2 0, B [0 0 1], (800 kV).

apart from the large stacking faults, there was only a very low density of teardrop-shaped perfect loops ($\sim 0.35\,\mu$m diameter). Annealing at 950° C for 17 h produced a lower density of large stacking faults which had, however, increased in size ($\lesssim 2\,\mu$m in diameter). There was also a very low density of perfect, parallelogram-shaped loops.

Specimens taken from region γX and examined in the as-received state and after annealing at 950° C for 17 h were found to contain large ($\lesssim 1.5\,\mu$m in diameter), complex faulted defects whose density was lower than that found in similarly treated specimens from region β. No background of small loops was observed in region γX.

No defect structure, apart from a very low density of grown-in dislocation lines, was observed in region γY, either in the as-received condition or after annealing at 950° C for 17 h. A–B etching and transmission electron microscopy revealed no defects in Slice A apart from grown-in dislocation lines. An analysis of the nature of the large, simple, single-layer faults in as-received and annealed material using the method of Gevers *et al.* [9] has shown them to be extrinsic in nature.

An analysis of the conveniently sized perfect loops in region α after annealing at 800° C using the method outlined by Maher and Eyre [10] suggests that they are near-edge and interstitial, with Burger's vectors of $a/2\langle 1\,1\,0\rangle$, while an analysis of the larger, parallelogram-shaped loops obtained in region α after annealing at 950° C suggests that these are interstitial with Burger's vector of $a/2\langle 1\,1\,0\rangle$ and lie close to either $\{1\,1\,0\}$ or $\{2\,1\,0\}$. Unlike the faulted and perfect loops observed in Te-doped GaAs [11] no evidence has been found for the existence of small precipitate particles on perfect and faulted loops in as-received or annealed Si-doped GaAs.

3.2. Zinc-diffused material

Zinc diffusions were carried out using a source with a composition of $Zn_{28}As_{72}$ [7] at 865° C for 4 h on material from region α. The source-weight to ampoule-volume ratio was $1.0 \pm 0.1\,\text{mg cm}^{-3}$. Fig. 4 is a montage from a transverse specimen showing the resultant variation in defect structure with depth. This can be most easily described by division into four regions (Fig. 4) which are broadly similar to those observed in Te-doped GaAs after an equivalent diffusion [7]. The relevant differences between the two cases are that in Si-doped GaAs there is still a low density (compared to Region ii) of large, circular stacking faults in Region (iii), that irregular line dislocations are observed in Regions (ii), (iii) and (iv), and that in Region (iv) there exists a high density of small precipitates showing Moiré fringes (Fig. 5) in the volume within 8 μm of the original surface. Apart from these differences, the diffusion-induced defect structure is the same as in similarly diffused, heavily Te-doped GaAs, in that precipitation and the growth of interstitial loops are observed in Region (ii) (Fig. 6), while at smaller depths the loop structure is observed to shrink (Region iii) before disappearing entirely (Region iv).

An analysis of the large perfect and faulted loops in Regions (ii) and (iii) using the methods of Maher and Eyre [10] and Gevers *et al.* [9], respectively, has found them to be identical to their counterparts in the annealed bulk.

High magnification of the precipitates formed

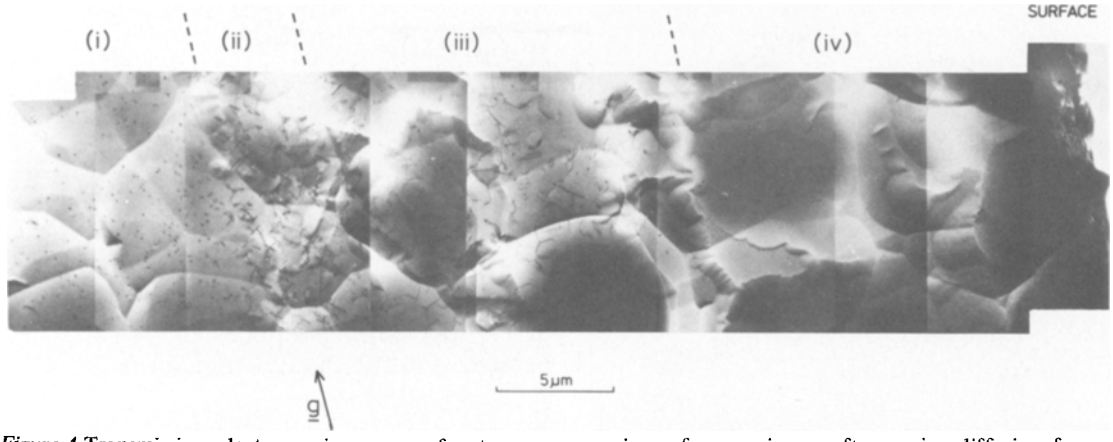

Figure 4 Transmission electron microscopy of a transverse specimen from region α after a zinc diffusion from a $Zn_{28}As_{72}$ source at a source-weight to ampoule-volume ratio of $1.0\,\text{mg cm}^{-3}$. Diffusion time 4 h and temperature 865° C; 800 kV electrons, $\mathbf{B} \sim [1\,1\,0]$, $\mathbf{g}\ 2\,\bar{2}\,0$.

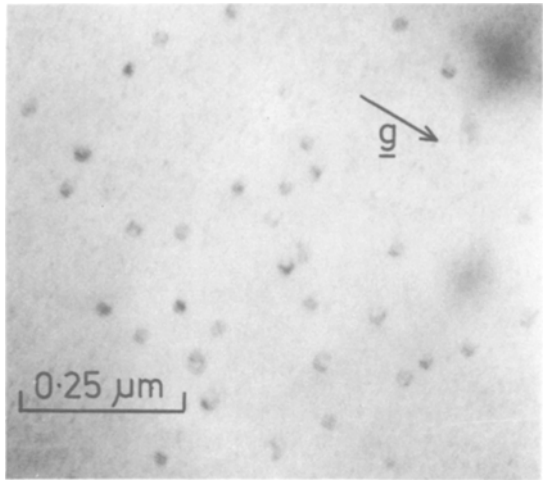

Figure 5 Small precipitates showing Moiré fringes observed in the surface region of a zinc-diffused specimen. g 2 2 0, **B** [0 0 1], (800 kV).

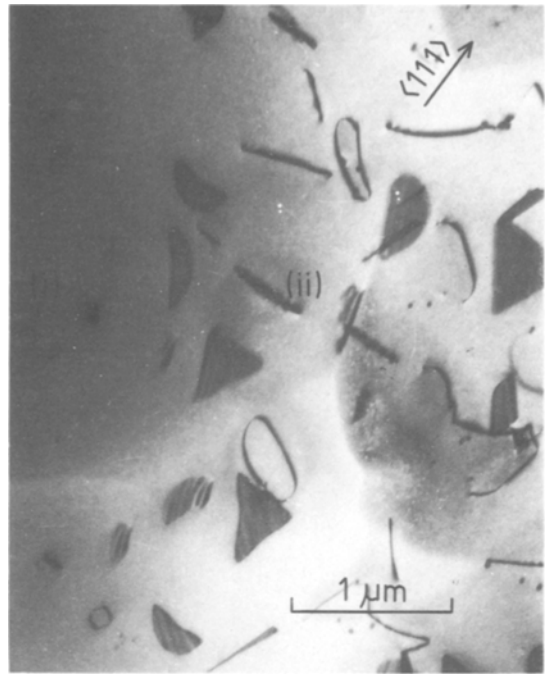

Figure 6 Large perfect and faulted loops and precipitation in Region (ii) of a zinc-diffused transverse specimen. The annealed bulk (Region i) is shown at the extreme left. g $\bar{1}$ 1 1, **B** [1 1 0], (800 kV).

in Region (ii) indicates that while in Region (ii) their contrast is suggestive of a spherical strain field, in Regions (iii) and (iv) they show only absorption contrast. Weak-beam microscopy also shows them to tend towards a tetrahedral shape in Regions (iii) and (iv) (Fig. 7). They also show asymmetry in that when using any ⟨1 1 2⟩ or ⟨1 1 0⟩ beam direction all the precipitates (which appear as triangles in this orientation) "point" in the same direction. Similar behaviour has been observed with tetrahedral precipitates in S-doped GaP [12].

Examinations of the precipitates which exhibit Moiré fringes in the surface region using the EDX facility and a beam of the same size as the precipitates has identified zinc as being present. No other species were detected apart from gallium and arsenic.

3.3. Copper-diffused material

Diffusions were carried out using sufficient pure copper as the source such that solid copper

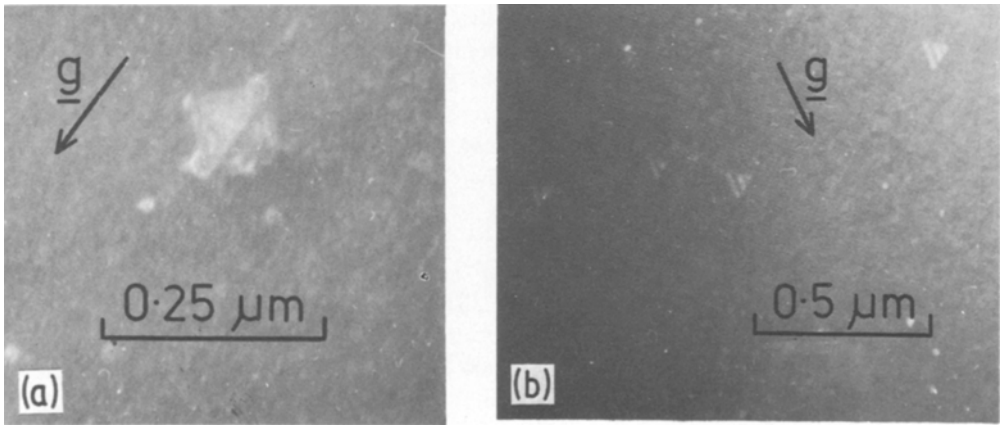

Figure 7 Precipitate particles formed in Region (ii) after zinc diffusion examined in Region (iv). They are revealed as (a) squares in the (0 0 1) projection (g 2 2 0, 800 kV, weak-beam, dark-field image); (b) triangles in the (1 1 0) projection (g 2 $\bar{2}$ 0, 800 kV, weak-beam, dark-field image). All triangles are observed to "point" in the same direction.

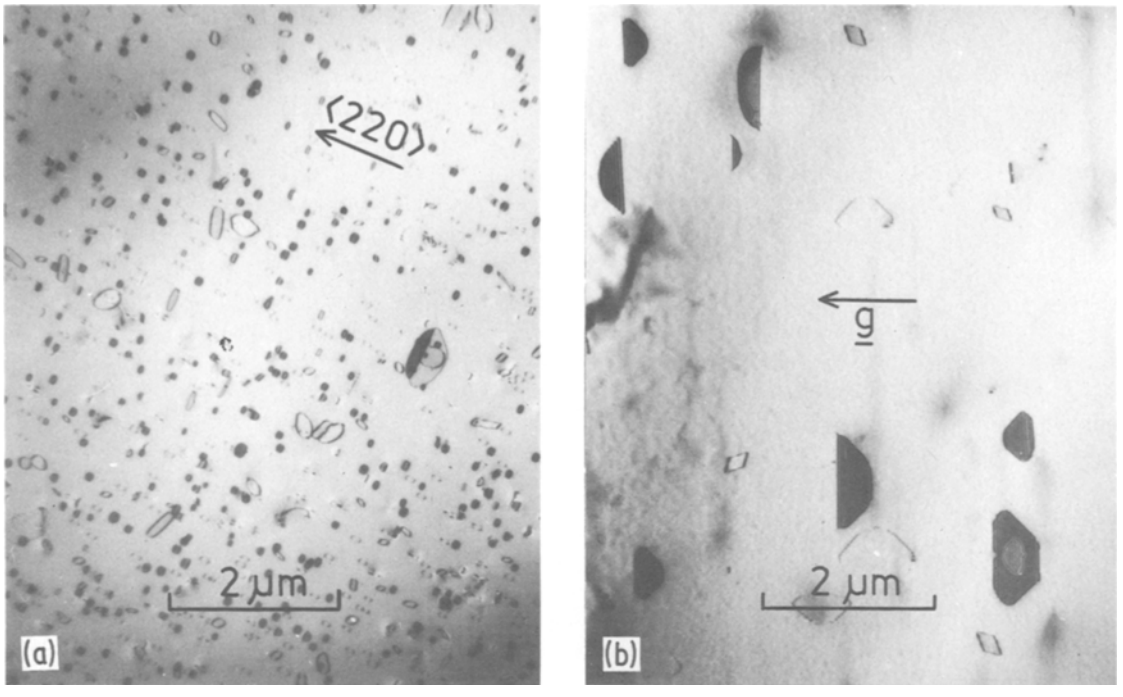

Figure 8 Faulted and perfect loops after copper diffusion in region α. (a) 850° C, 3 h, **g** 2 2 0, **B** [0 0 1], (800 kV); (b) 950° C, 3 h, **g** 2 $\bar{2}$ 0, **B** [0 0 1], (800 kV).

remained within the ampoule after quenching. Diffusion times varied from 1 to 3 h and transverse specimens indicated that the resultant defect structure was unaffected by depth. Fig. 8a and b show the results of copper diffusion in the α-region of slice B at 850° C and 950° C, respectively. Comparison with the annealing results (Table I) suggests that at 850° C, copper diffusion has caused both the density and area of the perfect and faulted loops to increase. Small precipitates are observed on most of the perfect loops after copper diffusion. Diffusion at 950° C produces large (edge length $\lesssim 1\,\mu m$) stacking faults and large, parallelogram-shaped, perfect loops. Both these are observed in equivalently annealed material except that the density of both is far greater in copper-diffused material. An analysis of the perfect and faulted loops using the methods outlined by Maher and Eyre [10] and Gevers *et al.* [9] respectively showed them to be identical to their counterparts in annealed-only material.

4. Discussion

4.1. As-received and annealed material

The precise level of silicon doping at any specific point on the two single-crystal slices used in these experiments was not known; however, the work of Darby [1] and Darby *et al.* [2] suggests that the "s"-pits observed after A–B etching and the loops observed in the transmission electron microscope do not appear until the silicon doping exceeds a certain level, and that the density of both increases with increasing silicon doping. This implies that, with reference to Fig. 1, regions α and δ correspond to the highest silicon doping, region γY to the lowest and regions β and γX to intermediate doping levels. The results of our examination of the defects present in slice B are largely in agreement with previous examinations [1, 3] of heavily and, comparatively, lightly silicon-doped substrate material. The correspondence between the defect structure and the doping level tends to imply that the silicon dopant is associated with the formation of the defects.

The results of annealing in region α in this investigation (Table I) suggest that annealing at 600° C produces an increase in both small faulted and perfect loop area while temperatures above 600° C and below 950° C produce an increased perfect loop area but a decreased small stacking-fault area as compared with 600° C. The results obtained are somewhat at variance with those of

a previous annealing study of heavily Si-doped GaAs by Narayanan and Kachare [3], in that these authors observed a decrease in the size of the perfect loops between 600° C and 750° C and also gave the nature of these loops as vacancy. There is, however, some agreement in that Narayanan and Kachare suggest that the density of perfect loops increases between 600 and 750° C and that their size increases and density decreases at 850° C relative to the 750° C anneal. The discrepancy at the lower temperature, 600° C, may be due to the differing thermal histories of the samples used in Narayanan and Kachare's experiments and in ours, but we remain in disagreement on the nature of the perfect loops.

If the perfect loops are interstitial then this implies that annealing at temperatures below 950° C produces interstitials and that increasing the temperature (below 950° C) produces further interstitials since the perfect loop area is observed to increase. A possible explanation for this can be found in the localized vibrational mode and free-carrier concentration measurements carried out by Kung and Spitzer [13] on annealed, heavily Si-doped GaAs. These authors pre-annealed all their specimens at 1100° C for 15 min, followed by quenching, in order to establish a common thermal condition for all their samples. Such specimens were subsequently annealed at three different temperatures, 400° C, 650° C and 750° C. Kung and Spitzer's results suggested that annealing at these temperatures produced no real change in the concentration of silicon on arsenic sites or (Si_{Ga}–Si_{As}) pairs but that the Si_{Ga} concentration altered with the annealing temperature, namely that, in comparison with the Si_{Ga} concentration after the 1100° C pre-anneal, it fell sharply at all three temperatures though the decrease was larger the lower the temperature. Kung and Spitzer [13] also found that when they compared the difference between the Si_{Ga} and Si_{As} levels which, assuming no other charged species, should give the free-carrier concentration, the resultant values were distinctly higher than the actually measured free-carrier concentration at annealing temperatures above 400° C but below 1100° C. Because of this they suggested that a model for the annealing effects requires two mechanisms; (a) a substantial decrease in the Si_{Ga} concentration (compared with the 1100° C pre-anneal) which is temperature dependent in the manner described above and observed at 400° C, 650° C and 750° C, and (b) generation of a substantial concentration of additional acceptors particularly at the higher annealing temperatures, but not at 1100° C. It was tentatively suggested that the defect responsible was the complex ($Si_{Ga}V_{Ga}$). It is suggested in the present work that the formation of these defects could explain the progressive rise in perfect loop area below 950° C since the formation of such defects would imply a fall in the gallium vacancy concentration which would therefore tend to induce Frenkel disorder on the gallium sub-lattice:

$$Si^{+}_{Ga} + V^{r-}_{Ga} = (Si_{Ga}V_{Ga})^{(n+r-1)-} + nh^{+}$$

$$Ga_{Ga} = V_{Ga} + Ga_i.$$

The resultant excess gallium interstitials could then either diffuse to already present perfect loops and cause growth by either a Petroff–Kimerling mechanism [14] or by pairing with arsenic interstitials (it having been suggested [15] that Frenkel disorder on the arsenic sublattice is dominant at these temperatures) or, alternatively, nucleate further interstitial perfect loops. Such a mechanism would also explain the increase in perfect loop area with annealing temperature below 950° C since Kung and Spitzer's [13] comparison of the expected free-carrier concentration, from the Si_{Ga} and Si_{As} levels, and the measured free-carrier concentration implies a progressive increase in the ($Si_{Ga}V_{Ga}$) concentration between 400 and 750° C. Equivalently this would also explain the sudden shrinkage of the perfect loops at 950° C since it is Kung and Spitzer's observation that no ($Si_{Ga}V_{Ga}$) complexes are observed after an 1100° C anneal, which suggests their disappearance at some temperature inbetween 750 and 1100° C.

Finally, the rise in the Si_{Ga} concentration with annealing temperature observed by Kung and Spitzer [13] could possibly be associated with the dissolution of the small stacking faults at temperatures above 600° C if these comprise layers of silicon on {1 1 1} planes. The larger stacking faults, which would also probably be composed of silicon, would be less affected since their greater size makes them more stable.

4.2. Zinc-diffused material

Diffusions using a $Zn_{28}As_{72}$ source at 865° C for 4 h at a source-weight to ampoule-volume ratio of $1.0 \pm 0.1\ mg\,cm^{-3}$ produce a diffusion-induced defect structure which varies with depth in a similar manner to that observed in Te-doped GaAs

diffused under equivalent conditions [7]. This tends to imply that the defect structures arise via the same mechanism particularly since both materials are found to contain interstitial perfect and faulted loops in both the annealed bulk and diffused regions. In Te-doped GaAs it was suggested that the growth of the interstitial loops at the diffusion front (Region ii) was due to the incorporation of zinc interstitials on to substitutional gallium sites arising from the dissociative [16, 17] mechanism of zinc diffusion in GaAs:

$$Zn_i^{n+} + V_{Ga} = Zn_{Ga}^{-} + (n+1)\,h^+.$$

This reaction, which is occurring at its maximum intensity at the diffusion front, could result in a local depletion of gallium vacancies and induce Frenkel disorder on the gallium sublattice in order to accommodate further zinc interstitials:

$$Ga_{Ga} = V_{Ga} + Ga_i.$$

Thus a likely consequence of zinc diffusion is the formation of excess gallium interstitials at the diffusion front [7, 17]. The diffusion of these to the perfect loops would, in combination with arsenic interstitials, produce growth by climb [7] or, alternatively, together with zinc interstitials, cause precipitation. This explanation seems likely to apply to the present case since, considering the results of Ball *et al.* [7] and Darby *et al.* [2], who reported an approximate correlation between the p–n junction and the maximum depth of the diffusion-induced dislocation structure in zinc-diffused Te and Si-doped GaAs respectively, Region (ii) would appear to correspond to the approximate position of the diffusion front.

There are, however, some differences between the Si-doped and Te-doped cases. Firstly the stacking faults in Si-doped GaAs cannot be composed of Ga_2Te_3, as has been suggested to be the case in Te-doped GaAs [7, 18]. However, it seems likely that they are composed of silicon since they are observed to preferentially dissolve, compared with the perfect loops, behind the diffusion front, a point which could be explained by an enhanced solubility of silicon donors in what is now p^+ material in order to supply compensating electrons. However, as compared with the stacking faults in Te-doped GaAs (for which a similar explanation was advanced [7]) those in Si-doped GaAs are observed to dissolve more slowly behind the diffusion front. This is possibly due to competition for gallium vacancies between the silicon in the stacking faults and the silicon on arsenic sites, which are acceptors and whose solubility is therefore likely to decrease in p^+ material. The original growth of these stacking faults at the diffusion front could arise from the incorporation of zinc:

$$Si_{Ga}^{+} = Si_i + V_{Ga} + h^+$$

$$Zn_i^{r+} + V_{Ga} = Zn_{Ga}^{-} + (r+1)\,h^+.$$

Another difference between the Si-doped and Te-doped zinc-diffused materials is the appearance of zinc-rich precipitation close to the surface in Si-doped material. This is thought to be a consequence of the amphoteric [19] nature of silicon in GaAs in that it is close to the diffusion surface that the substitutional zinc concentration is highest and, therefore, where the solubility of silicon acceptors on arsenic sites is, presumably, at its lowest. Thus it is close to the surface that the silicon on arsenic sites and zinc interstitials are likely to be most in competition for gallium vacancies. Since the incorporation of silicon on to a gallium vacancy provides a compensating electron whereas zinc provides a positive hole it is perhaps not surprising in p^+ material that it is the zinc which precipitates out of solution.

Finally, in Te-doped and Si-doped GaAs, it is observed that zinc diffusion under these conditions produces a region denuded of dislocation loops extending in from the surface. In Te-doped GaAs it was argued [7] that this was partly due to the situation being closer to equilibrium with respect to the gallium vacancies behind the diffusion front, such that those gallium interstitials formed at the diffusion front could now diffuse away from the perfect loops. However, since this would have been expected to result in smaller loops, rather than their complete dissolution, an additional mechanism had to be invoked. It was suggested that the defect responsible for the formation of interstitial loops in Te-doped GaAs, which it is thought [15] is $(Te_{As}V_{Ga})^-$, being an acceptor, becomes unstable in p^+ material and breaks up. In so doing it provides a gallium vacancy which enables the perfect loops to completely dissolve. Since the loop structure in zinc-diffused Si-doped material is also completely removed in a region extending in from the surface, this implies that a similar situation is occurring to that in Te-doped GaAs with perhaps the $(Si_{Ga}V_{Ga})$ complex, suggested as being present from the annealing results, taking

the place of the $(Te_{As}V_{Ga})^-$ complex. If so, this would tend to imply that the $(Si_{Ga}V_{Ga})$ complex is either an acceptor or neutral.

Electron micrographs of the defect structure of heavily Si-doped GaAs after zinc diffusion have previously been published by Darby *et al.* [2]. Though the exact diffusion conditions are not specified, examination of the defect structure shows the same trends observed in this work. Namely the growth of perfect and faulted loops near the p–n junction, the shrinkage behind this and a denuded region extending in from the surface.

4.3. Cooper-diffused material

Copper, like zinc, is thought to diffuse very rapidly in the interstitial form in GaAs before becoming relatively immobile as an acceptor on the gallium sublattice [20]. When copper is diffused at 850 and 950° C into Si-doped GaAs, which contains a high background density of perfect and faulted loops (region α), a substantial increase in the perfect and faulted interstitial loop area is observed (Table I). An increase in the perfect loop area is also observed after copper diffusion into Te-doped GaAs [21]. It therefore seems probable that the same mechanism of perfect loop growth is operating in both cases. It is suggested here that this is due to the incorporation of copper interstitials on to vacant sites on the gallium sublattice. This would lower the gallium vacancy concentration and could, therefore, promote Frenkel disorder in order to accommodate further copper interstitials:

$$Ga_{Ga} = V_{Ga} + Ga_i.$$

The diffusion of the gallium interstitials to the perfect loops would then cause growth by climb in a similar manner to that argued for the growth of perfect loops during zinc diffusion. The growth of such loops in copper and zinc-diffused Te-doped and Si-doped GaAs due to the formation of gallium interstitials tends to imply that either the original arsenic interstitial concentration is higher than the gallium interstitial concentration or that arsenic interstitials are easily formed under these conditions. As regards the faulted loops in Si-doped GaAs, other results in this work tend to suggest that they are composed of silicon. Thus their growth in copper-diffused material could either be due to the generation of silicon interstitials from the gallium sublattice in the same manner as gallium interstitials (i.e. the in-diffusing copper interstitial effectively displaces silicon donors from gallium sites) or, since substitutional copper is an acceptor in GaAs, that the solubility of silicon acceptors on the arsenic sites is reduced with the result, since they are in direct competition with the faster diffusing copper for gallium vacancies, that they precipitate out on the stacking faults.

5. Conclusions

The results presented on as-received material are broadly in agreement with those of previous studies in that the type and density of the defect structure is found to be dependent on the silicon doping level. The majority of defects in the heavily doped materials are found to be small faulted and perfect dislocation loops. The results of annealing this structure show that, below 950° C, there is a progressive rise in perfect loop area with temperature while the small stacking faults show an initial rise in area at 600° C but a marked fall at temperatures above this. Above 950° C the area of both is extremely small. These trends have been interpreted in terms of the localized vibrational mode (LVM) and free-carrier concentration measurements carried out by Kung and Spitzer [13] on annealed Si-doped GaAs in that the growth and shrinkage of the perfect, interstitial loops have been linked with the formation and dissolution of the compensating complex $(Si_{Ga}V_{Ga})$, while it has been suggested that the shrinkage of the small stacking faults above 600° C is responsible for the observed increase in the silicon donor concentration [13] at these temperatures.

The results of the zinc diffusions into heavily Si-doped GaAs have been found to be very similar to those observed after equivalent diffusions into Te-doped GaAs [7]. Using a source with a composition of $Zn_{28}As_{72}$ at 865° C has been found to result in interstitial loop growth at the suspected diffusion front, while behind this, progressive dissolution of the loop structure occurs. It has been suggested that the growth of the loops can be attributed to the dissociative mechanism of zinc diffusion which will reduce the gallium vacancy concentration at the diffusion front. This may then induce Frenkel disorder on the gallium sublattice with the consequent excess gallium interstitials causing loop growth. The dissolution of the loop structure has been attributed to the closer-to-equilibrium situation with respect to the gallium vacancies operating behind the diffusion front, together with the change in electrical character

of the material and its effect on the stability of the ($Si_{Ga}V_{Ga}$) complex.

The results of the copper diffusion into heavily Si-doped material show a large increase in both perfect and faulted loop area compared to equivalently annealed specimens. The growth of the perfect loops has been attributed to the diffusion mechanism of copper in GaAs in an analogous fashion to that of loop growth during zinc diffusion. The growth of the faulted loops is probably due either to the formation of silicon interstitials from the gallium sublattice, in a similar fashion to that suggested for the gallium interstitials, or to the decreased solubility of silicon acceptors on arsenic sites because of the compensated or p-type nature of diffused material.

Finally some workers have analysed the perfect loops in Si-doped GaAs as being vacancy in character [3, 22]. However, since the accepted model for the incorporation mechanism of zinc during diffusion into GaAs requires the elimination of gallium vacancies near the diffusion front, vacancy loops would be expected to shrink at this point. This is contrary to the observation in this work that the perfect loops grow at the suspected diffusion front.

Acknowledgements

The authors acknowledge the financial support of both the Ministry of Defence DCVD and the Science Research Council. We are grateful to Professor R. E. Smallman for the provision of laboratory facilities, to Dr P. S. Dobson for continued encouragement and to Dr I. P. Jones for assistance with the EDAX facility and useful discussions.

References

1. D. B. DARBY, DPhil. Thesis, Oxford University, Department of Metallurgy and Science of Materials (1979).
2. D. B. DARBY, P. D. AUGUSTUS, G. R. BOOKER and D. J. STIRLAND, *J. Microsc.* **118** (1980) 343.
3. G. H. NARAYANAN and A. H. KACHARE, *Phys. Stat. Solidi (a)* **26** (1974) 657.
4. D. GREENE, private communication (1980).
5. R. NEWMAN, private communication (1980).
6. M. S. ABRAHAMS and C. J. BUIOCCHI, *J. Appl. Phys.* **36** (1965) 2855.
7. R. K. BALL, P. W. HUTCHINSON and P. S. DOBSON, *Phil. Mag.* **43** (1981) 1299.
8. D. J. STIRLAND, private communication (1980).
9. R. GEVERS, A. ART and S. AMELINCKX, *Phys. Stat. Solidi* **3** (1963) 1563.
10. D. M. MAHER and B. L. EYRE, *Phil. Mag.* **23** (1971) 409.
11. P. W. HUTCHINSON and P. S. DOBSON, *ibid.* **38** (1978) 15.
12. R. K. BALL and P. W. HUTCHINSON, *J. Mater. Sci.* **15** (1980) 2376.
13. J. K. KUNG and W. G. SPITZER, *J. Appl. Phys.* **45** (1974) 4477.
14. P. M. PETROFF and L. C. KIMERLING, *Appl. Phys. Lett.* **29** (1976) 461.
15. D. T. J. HURLE, *J. Phys. Chem. Solids* **40** (1979) 627.
16. R. L. LONGINI, *Solid State Elect.* **5** (1962) 127.
17. H. R. WINTELER, *Helv. Phys. Acta* **14** (1971) 451.
18. P. W. HUTCHINSON and P. S. DOBSON, *Phil. Mag.* **30** (1974) 361.
19. W. G. SPITZER and W. ALLRED, *J. Appl. Phys.* **39** (1968) 4999.
20. R. N. HALL and J. H. RACETTE, *ibid.* **35** (1964) 379.
21. P. W. HUTCHINSON and P. S. DOBSON, *J. Mater. Sci.* **10** (1975) 1636.
22. V. SWAMINATHAN and S. M. COPLEY, *J. Appl. Phys.* **47** (1976) 4405.

Received 1 May
and accepted 3 July 1981